Neuroscience 120 (2003) 1061–1069

INTRINSIC COLLATERALS OF LAYER 6 MEYNERT CELLS AND FUNCTIONAL COLUMNS IN PRIMATE V1

H. LI,[1] M. FUKUDA,[2] M. TANIFUJI AND K. S. ROCKLAND*

RIKEN Brain Science Institute, 2-1 Hirosawa, Wako-shi, Saitama, Japan 351-0198

Abstract—Meynert cells are a distinct type of large neuron which project to area MT/V5 and to subcortical targets, including the superior colliculus. They have recently been shown to have extensive intrinsic collaterals spreading up to 8.0 mm within layer 6 of area V1 [J Comp Neurol 441 (2001) 134]. Using intrinsic signal imaging combined with tracer injections, this study investigates how Meynert cell collaterals are mapped in relation to the functional architecture of area V1 in macaque monkeys. In particular, we examined whether terminations of individual axon segments are selective for same-eye or opposite-eye domains. Analysis of 39 anterogradely labeled axon segments (from six injection sites in four hemispheres) showed that terminal segments cross over several pairs of ocular dominance columns (ODCs) and contact both left- and right-eye ODCs, with a slight bias for the contralateral eye. This contrasts with the same-eye bias previously reported for intrinsic collaterals of pyramidal neurons in layer 3. The suggestion is that the system of Meynert intrinsic collaterals is involved with binocular interactions over wide sectors of the visual field. This might be related to processes such as optic flow or, especially given the wide-field spread, even contour completion or interpolation.

Key words: area MT/V5, binocular, horizontal connections, infragranular layers, ocular dominance columns, optical imaging.

A basic tenet of cortical organization is that primary sensory areas have functionally modular domains arranged within topographically ordered representations. Modularity has been repeatedly demonstrated by techniques such as 2-deoxyglucose and, more recently, intrinsic signal imaging and fMRI (Blasdel and Salama, 1986; Ts'o et al., 1990; Grinvald et al., 1991; Blasdel, 1992; Cheng et al., 2001; and references therein). In the primary visual cortex of primate, the classical hypercolumn has been designated as a basic unit about 1.0 mm wide, which represents all orientations through one right- and left-eye pair of ocular dominance columns (ODCs; Hubel and Wiesel, 1968, 1977).

ODCs are known to be closely associated with the pattern of geniculocortical terminations (Hubel and Wiesel, 1972; Blasdel and Lund, 1983), but in addition to thalamocortical connections, several other connectional systems have been shown to have an orderly relationship to the functional architecture of area V1. These include neurons projecting to extrastriate cortical areas (Livingstone and Hubel, 1983; DeYoe and Van Essen, 1988; Zeki and Shipp, 1989: Boyd and Casagrande, 1999; Sincich and Horton, 2002, among others), and the intrinsic terminal patches formed by horizontal collaterals of pyramidal neurons in layers 3 and 4B (Rockland and Lund, 1983; Yabuta and Callaway, 1998; Stettler et al., 2002, and references therein). Several investigations have shown that these intrinsic patches, visualized by tracer injections, interconnect same eye domains (Malach et al., 1993; Yoshioka et al., 1996; Stettler et al., 2002).

Recently, another system of very divergent intrinsic connections, extending up to 8.0 mm, has been reported to originate from Meynert cells in layer 6 (Rockland and Knutson, 2001). Meynert cells are a specialized class of large cells, like Betz cells in the motor cortex. They are known to project to both area MT/V5 and the superior colliculus, often via branched collaterals (Fries et al., 1985; Vogt Weisenhorn et al., 1995); are thought to be involved in the motion detection system (Movshon and Newsome, 1996); and their cell bodies are reported to lie preferentially beneath the low cytochrome oxidase (CO), interpatch regions of layer 3 (Payne and Peters, 1989). Given their functional and anatomical specializations, we wanted to ascertain first, whether Meynert intrinsic collaterals, like the supragranular intrinsic connections, had any discernible relationship to the basic modularity in V1; and second, whether, like their parent cell bodies, they might be situated below the CO interpatch matrix, corresponding to the binocular edges of ODCs. For this purpose, we visualized the ODCs by intrinsic signal imaging, placed injections of anterograde tracers at defined sites within the imaged maps, and subsequently carried out reconstructions of selected Meynert segments to align these with the pre-imaged ODCs. Preliminary results have been presented in abstract form (Li et al., 2000, 2001).

EXPERIMENTAL PROCEDURES

Animals

Three adult rhesus monkeys (*Macaca mulatta*) were used for combined intrinsic signal imaging and axonal tracing analysis. In one of these (R19), both hemispheres were used, in order to

[1] Present address: Neurosurgery Research Laboratories, State University of New York Health Science Centre at Syracuse, 750 East Adams Street, Syracuse, NY 13210, USA.
[2] Department of Neurobiology, University of Pittsburgh, McGowan Institute of Regenerative Medicine, Brain Imaging Research Center, 3025 East Carson Street, Pittsburgh, PA 15203, USA.
*Corresponding author. Tel: +81-48-467-6427; fax: +81-48-467-6420.
E-mail address: rockland@brain.riken.go.jp (K. S. Rockland).
Abbreviations: BDA, biotinylated dextran amine; CO, cytochrome oxidase; DiI, 1,1′-dioctadecyl-3,3,3′,3′-tetramethylindocarbocyanine perchlorate; EEG, electroencephalographic; FR, Fluoro Ruby; ODC, ocular dominance column; PB, phosphate buffer.

0306-4522/03$30.00+0.00 © 2003 IBRO. Published by Elsevier Ltd. All rights reserved.
doi:10.1016/S0306-4522(03)00429-9

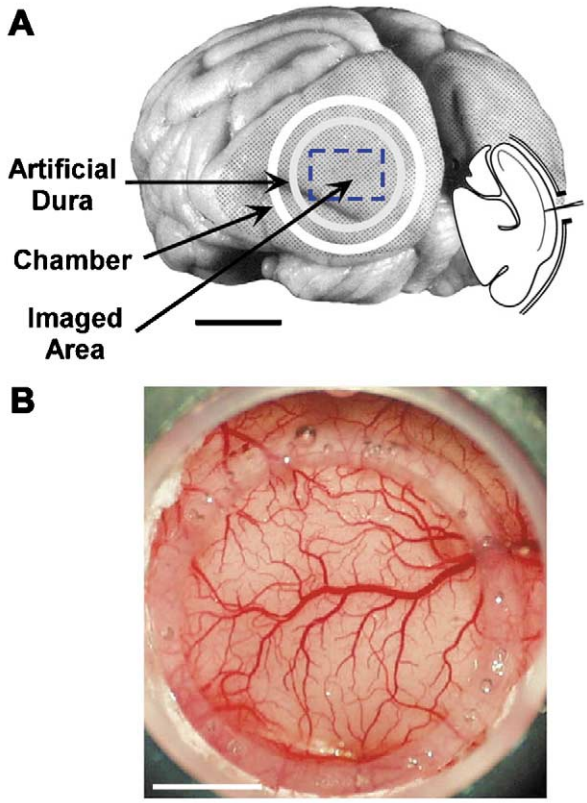

Fig. 1. Experimental setup for optical imaging. (A) A chamber is implanted, dura excised, and artificial dura substituted over the region exposed for optical imaging (blue rectangle). The coronal section insert at right (from a right hemisphere) schematically depicts the approximate position of the implanted chamber and the distal portion of an injection pipette. (B) View of the exposed cortical surface taken with a digital camera immediately after an optical imaging session. Scale bars in A=1 cm, in B=5 mm.

minimize the number of animals necessary for this study. Imaging was carried out in the dorsal operculum of V1 (lower visual field representation, at approximately 6–10°; see Fig. 1A). Care was taken to avoid discomfort to the monkeys; and all surgical procedures were approved by the animal experimental committee of RIKEN, and conformed to the National Institutes of Health (USA) guidelines.

Optical recording of intrinsic signals

A week before recording, we performed aseptic surgery, with pentobarbital anesthesia (25 mg/kg, i.v.), in order to implant on the skull a stainless steel post for head fixation; two screw bolts for electroencephalographic (EEG) monitoring; and a chamber for optical imaging (inner diameter of 19 mm; outer, 25 mm; Fig. 1A).

On the day of optical recording, the monkey was anesthetized initially with ketamine hydrochloride (10 mg/kg) and then with a gas mixture of isoflurane and a mixture of 70% N_2O and 30% of O_2. The monkey was paralyzed by pancuronium bromide or vecuromium bromide and artificially ventilated. Contact lenses were fit to the eyes, and images at 57 cm from the cornea were focused on the retina. The rectal temperature and expired CO_2 were monitored; and temperature was maintained at 37.0 °C, and expired CO_2, at between 4.5 and 5.0%. Electrocardiogram and EEG were also monitored throughout the experiment.

Craniotomy and partial durotomy were carried out under strict sterile conditions. An artificial dura (Shtoyerman et al., 2000) was

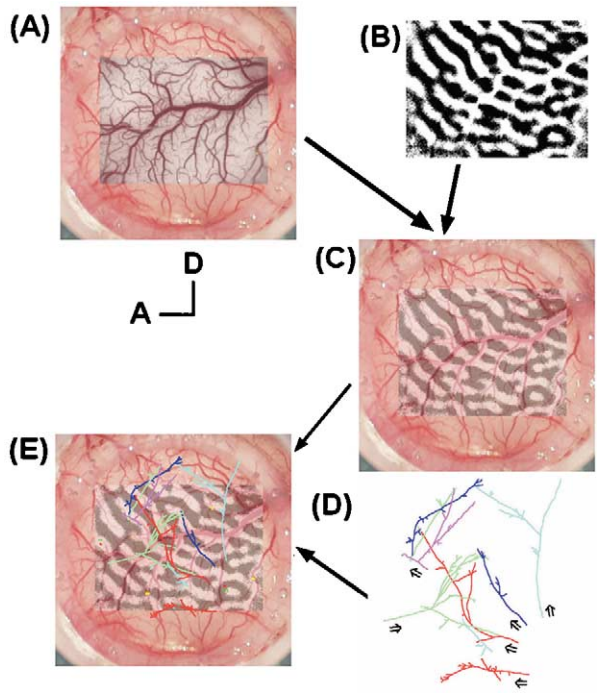

Fig. 2. Illustration of five steps in the alignment process (from monkey 19, left hemisphere). A) The surface blood vessel pattern is photographed with a CCD camera in 570 nm illumination. This image (8.8×6.6 mm) is aligned with the digital image (as seen in A, in the lower color layer). B) The ODC map is obtained by monocular visual presentation of square waves in four orientations. C) The ODC map is superimposed as another layer on the cortical surface image (same as in A); and coordinates are chosen relative to the blood vessel pattern to target tracer injections within identified left- or right- eye ODCs. D) After perfusion and histological processing, anterogradely labeled Meynert segments (arrows point to six of 10 segments shown from monkey 19; see also Fig. 6A), are identified and traced through serial sections within and immediately surrounding the imaged area in V1. E) The completed reconstructions are reduced in scale and aligned with the pattern of ODCs, using previously injected DiI spots (3 yellow dots in E) and the surface vasculature as enregistering landmarks (see Experimental Procedures). Scale bar, A–C, E=6 mm.

inserted between the remaining dura mater and the cortical surface to retard tissue regrowth (Fig. 1A). Subsequently, the chamber was filled with sterilized silicon oil (M.W. 1000; Shin-Etsu Chemical Co., Tokyo, Japan), and sealed with a glass cover.

For imaging, we used a video camera (CS8310; Tokyo Electronic Industry, Tokyo, Japan), and an IBM/PC-compatible computer equipped with a video frame grabber board (Pulsar; Matrox, Quebec, Canada; Tsunoda et al., 2001). The cortical surface vessels were viewed at 540 nm at the outset, and these images were later used for the alignment with the reconstructed Meynert segments (see below). The imaged area was 8.8×6.6 mm and contained 320×240 pixels. For imaging intrinsic signals, the wavelength of illumination was switched to 605 nm; and sequential images, at 600–700 μm below the cortical surface, were captured from 1 s before the stimulus onset for 4 s. The stimuli for each eye consisted of moving black and white gratings (0.5° black or white phase, drifting at 1°/s; duration, 2 s) that were presented on a TV monitor placed at 57 cm from the monkey's cornea. Four gratings of orientations 0°, 45°, 90° and 135° with respect to horizontal were presented in random order. The inter-stimulus interval was 10 s. Data were acquired during 20 presentations of each stimulus. Computer controlled shutters in front of each eye allowed monocular stimulation.

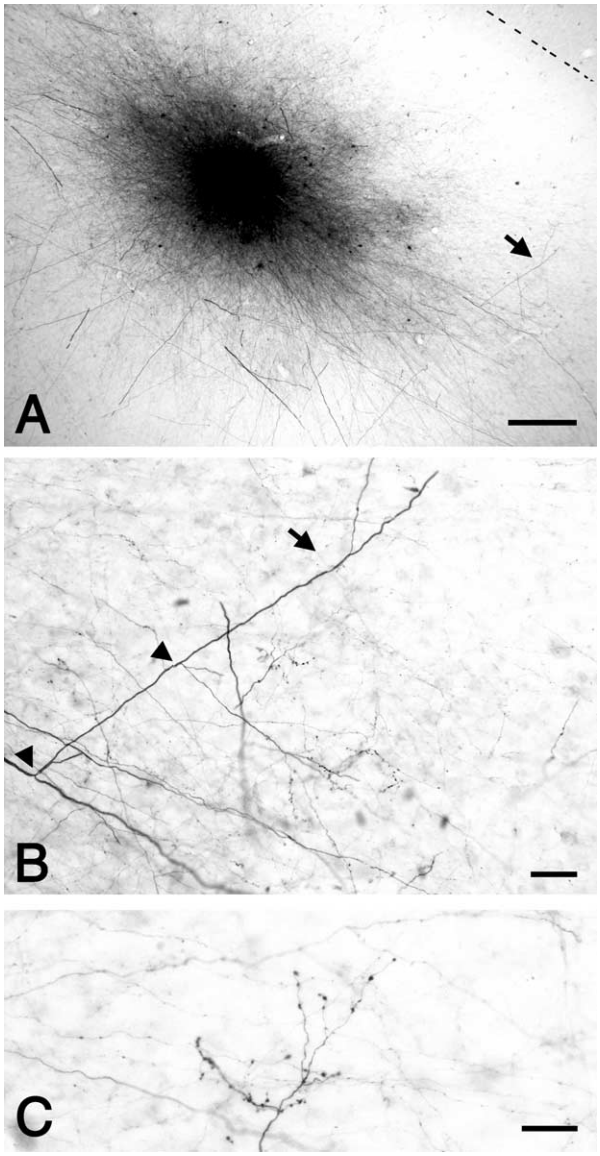

Fig. 3. Injection site and resulting label. A) Injection of BDA (from R22) in layer 6. Anterogradely labeled thick axon segments, characteristic of Meynert cell axons, exit from the injection site. Dashed line indicates bottom of layer 4C. (In the tangential plane, layer 4C also lies dorsal to the injection.) Arrow points to anterogradely labeled segment typical of Meynert cell collaterals. B) Higher magnification of Meynert collateral (arrows in A and B mark corresponding features). Four branches are apparent (two at lower arrowhead, one at upper arrowhead, and one at the arrow). C) Higher magnification of a Meynert-like terminal segment (beyond the arrow in A). Scale bars, A=100 μm, B=50 μm, C=30 μm.

Analysis of intrinsic signals

The spatial pattern of ODCs was obtained in the following way: (1) a differential image was obtained by dividing the averaged images obtained at 0.5–2.5 s after the stimulus onset, by those obtained during the 1-s period before the stimulus onset; (2) a Gaussian spatial filter was used to remove stimulus non-specific darkening and high-frequency noise of the differential image (cutoff frequency σ=20.4/mm for high cut, and σ=0.3/mm for low cut); and (3) the differential images obtained for all four orientations with one eye were averaged and subtracted from the equivalent average obtained for the other eye.

Tracer injection and axon reconstruction

In a separate surgical procedure, about 1 week after the optical imaging, biotinylated dextran amine (BDA) and/or Fluoro Ruby (FR; Molecular Probes, Inc., Eugene, OR, USA) were injected in order to anterogradely label axons in V1. BDA was dissolved at 10% concentration in 0.0125 M phosphate buffer (PB), and FR at 10% in 0.1 M PBS. Both tracers were used in cocktail (1:1; 3000:10,000 M.W). Of the four optically imaged hemispheres, two were injected with BDA only, and two with both BDA and FR into opposite ODCs. Injection location was targeted to the center of a left or right ODC, in reference to the pattern of surface blood vessels. Tracers were delivered iontophoretically (7 μA, in a 7 s ON/OFF cycle; 15–20 μm pipette tips) for 15–20 min in each site, at a depth of 0.8–1.0 mm. These parameters produced injections that were about 0.25–0.40 mm in base diameter. Injections were cylindrical in shape through layers 3–6, probably because some tracer spread along the pipette track. To aid in the alignment of the two datasets (labeled axons and optically imaged patterns), 1,1′-dioctadecyl-3,3,3′,3′-tetramethylindocarbocyanine perchlorate (DiI, Molecular Probes; 10%, in dehydrate ethanol) was pressure injected at three sites.

One week after tracer injection, monkeys were anesthetized with Nembutal (50 mg/kg, i.p.) and perfused transcardially, in sequence, with 0.5 l of 0.9% sodium chloride and 0.5% sodium nitrite; 4 l of 4% paraformaldehyde; and chilled 0.1 M PB with 10% and 20% sucrose (0.5 l each). As a final step, 30% sucrose PB with 0.5% nigrosine (Sigma, St. Louis, MO, USA) was perfused through the animal. This procedure resulted in black to grayish staining of the surface vasculature, and further aided in enregistering the blood vessel pattern of the optically imaged and the perfused brain. For histological processing, brains were cut in the tangential plane by frozen microtomy, at 50 um, and reacted in avidin–biotin complex (Vector Laboratories, Burlingame, CA, USA; Elite ABC kits). For single injections of BDA, tracer was visualized (see Rockland and Knutson, 2001) by a final histochemical reaction for DAB, with the addition of nickel ammonium sulfate (yielding a black color). When there was a second injection of FR, we continued by incubating the same sections for 2 days with anti-FR (1:600; Molecular Probes), biotinylated secondary antibody, and ABC-DAB. By not adding nickel, the final reaction product remained brown, and was easily distinguishable from the BDA-labeled processes.

The three DiI sites and injection site(s) were identified under the microscope, and digitized images were captured and aligned with the photograph of the optically imaged area (see below and Fig. 2). Labeled elements within this region were chosen for serial axon reconstruction. Reconstruction was carried out at 40×, 200×, 400×, and/or 1000× (for detailed identification). Meynert cell collaterals were easily identified, using several previously identified criteria (Rockland and Knutson, 2001; and see Results). Layer 6 was easily identified, as being more cell dense than either the overlying layer 5 or the subjacent white matter.

Alignment of functional column maps and Meynert cell collaterals

Precise alignment of the functional columns and the reconstructed axon segments is critical for our results, and we took several steps to aid in the accuracy of the alignment. First, care was taken to document the surface vasculature in several formats, both by digital camera (Olympus C-1400XL) and by CCD camera (570 nm; “green image”). This allowed us to co-register the vessels used as landmarks in the optical imaging session, in the injection placement, in the perfused brain, and in tangentially cut histological sections. Second, we used nigrosin in the perfusion

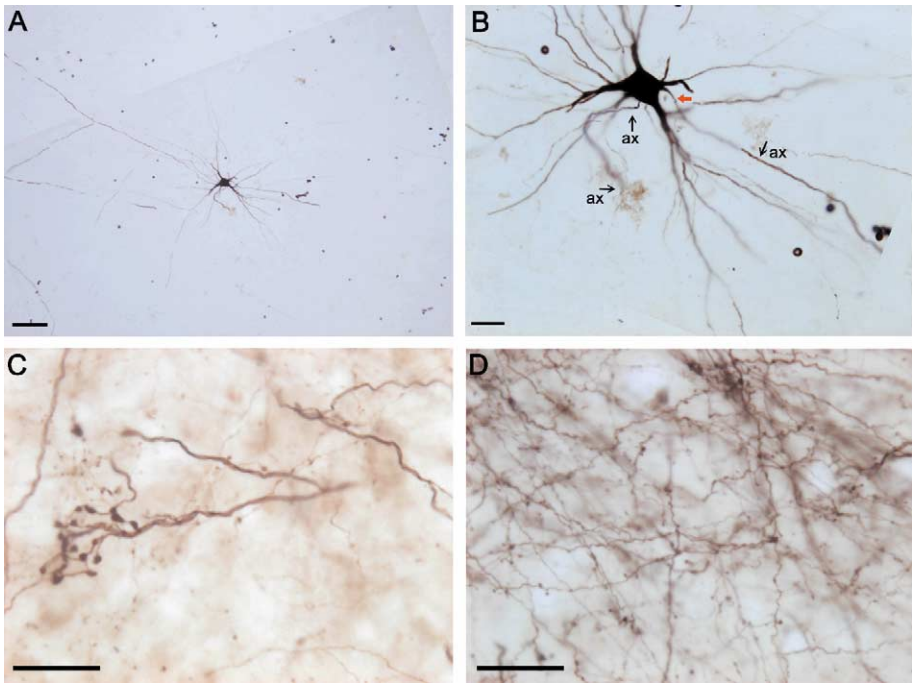

Fig. 4. Identifying characteristics of Meynert collaterals. A) An example of a retrogradely filled Meynert cell (from case 7, in Fig. 8, Rockland and Knutson, 2001), with portions of its dendritic arbor and axonal collaterals (Photoshop merge of two sequential sections). B) Higher magnification shows proximal portions of the axon as it exits the neuron in a dorsal location (see red arrow), and continues dorsally and toward the white matter (indicated by "ax" and arrows; the proximal bifurcation of the axon is obscured by the cell body). C) A typical small cluster of large boutons, deriving from a Meynert collateral. D) In contrast, a field of smaller boutons originating from pyramidal neurons in layer 3. Scale bars, A=150 um, B=25 um, C and D=50 um. Ax, axon.

fluid so as to enhance the contrast of the surface vessels in the perfused brain. Third, we placed three DiI spots in the living brain in relation to the surface vasculature. These spots were retrieved in the histological sections and, with the injection site, were used to confirm or adjust the alignment. The actual alignment was accomplished using Adobe Photoshop.

Pitfalls

Several possible technical problems need to be taken into account in interpreting these results. One is whether the identification of the axon segments as deriving from Meynert cells is valid. The strongest criterion for identification is to establish continuity between parent Meynert cells and the putative Meynert collaterals. We have achieved this for 12 cells ($n=10$, Rockland and Knutson, 2001; $n=2$, present study). Given the highly distinctive signature features of the collaterals (see Results), we are confident of our identifications even without demonstrating the parent neuron. A second problem is that our segments represent only part of the full collateral tree; and in particular we cannot rule out the possibility that several of the segments in our sample actually derive from the same neuron. While it would be more satisfying to have data for the entire collateral tree, we are confident that the trends, as such, are valid. Third, because parent cells are usually obscured within the injection site, it is not possible to know their exact location relative to center or edge of a particular ODC. A fourth, related issue is whether segments are truly labeled by anterograde transport from the injection site. This was evaluated in part by the orientation and configuration of individual segments in relation to the injection site (Fig. 3). In addition, there were only a few retrogradely filled Meynert cell bodies beyond the halo of the injection site (in contrast with large injections); and labeling did not extend into either the dendritic or axonal portions.

Fifth, and perhaps most important, is the accuracy of our alignment. Despite the precautions described above, small distortions may be introduced in extrapolating between the ODC pattern in layer 4 and the axon segments in layer 6. As a control for this possibility, we tested small shifted deviations in the alignment. This approach yielded the same conclusion; namely, that terminal segments were located in both ipsi- and contralateral ODCs.

RESULTS

Intrinsic signal imaging yielded the characteristic maps of ODCs (Fig. 2), consistent with results previously reported by other laboratories (e.g. Blasdel and Salama, 1986; Ts'o et al., 1990; Grinvald et al., 1991; Malach et al., 1993; Blasdel, 1992) After optical imaging, the monkeys were recovered, and data were analyzed off-line to choose injection targets. Ocular dominance was selected as a marker for functional architecture because it yields a robust signal, because it has been widely used as a standard map in other studies, because the optically imaged signal (focused at 600–700 μm below the cortical surface) is closer to layer 6 than are the CO patches in layer 3, and because CO histochemistry is not easily compatible with serial section axon analysis.

In a second procedure, we visualized Meynert collaterals by making iontophoretic injections of BDA and FR. These were placed in relation to the previously mapped ODCs (see Experimental Procedures). Injections were intended to remain within a single ODC, and measured

Table 1. Number of terminal boutons and distribution relative to ODCs

Monkey #	Axon #	Left ODC boutons	Right ODC boutons	Total number of boutons
#18	B1	10	16	26
Left V1	B2	3	0	3
	B3	73	40	113
INJ (BDA)	B4	30	9	39
Right ODC	B5	12	12	24
	B6	3	6	9
INJ (FR)	F1	34	6	40
Left ODC	F2	24	23	45
	F3	7	60	67
	F4	3	48	51
#22	B1	121	141	262
Right V1	B2	14	37	51
	B3	0	38	38
INJ (BDA)	B4	31	80	111
Left ODC	B5	17	163	180
	B6	7	14	21
	B7	0	4	4
	B8	0	19	19
#19	B1	155	67	222
Right V1	B2	47	42	89
	B3	25	110	135
INJ (BDA)	B4	26	240	266
Left ODC	B5	21	18	39
	B6	84	46	130
	B7	0	38	38
#19	B1	5	33	38
Left V1	B2	51	64	115
	B3	12	31	43
INJ (BDA)	B4	30	5	35
Left ODC	B5	9	4	13
	B6	94	8	102
INJ (FR)	F1	325	249	574
Right ODC	F2	11	27	38
	F3	0	17	17
	F4	18	20	38

0.25–0.40 mm in diameter in the dimension parallel to the pia (Fig. 3).

Injections produced a distinctive labeling pattern in layer 6. This consisted of thick axon segments, intermingled with relatively small terminal clusters ($d \leq 100$ μm), each of which carried a small number of relatively large boutons (up to 3.0 μm). The small clusters, large boutons, and thick axons all differ from intrinsic collaterals in the supragranular layer (Figs. 3, 4), and in a previous study were shown to originate from Meynert cells (Rockland and Knutson, 2001). In this study, the parent somas were ordinarily obscured within the injection site.

We reconstructed 44 axon segments from six sites, injected with BDA (reacted as black) or FR (reacted as brown), in four hemispheres of three monkeys (Table 1). Of these 44 axon segments, 39 are localized within the imaged regions (but four had no terminal clusters along the portion within the imaged area). Fig. 5 illustrates reconstructions of five segments labeled by a BDA injection placed in the center of a left ODC. All five segments arborised in layer 6, for distances up to 5.0 mm. Each segment bears small terminal clusters, with a variable center-to-center spacing, that ranged from 250 μm to 750 μm between clusters. Unlike supragranular intrinsic labeling, the layer 6 label was not dense and, in particular, did not converge in distinct patches.

Correlation of terminal clusters and ODC

The main goal in these experiments was to investigate how Meynert collateral segments mapped onto the functionally defined ODCs in V1. Fig. 6A and 6B shows respectively 10 and eight axon segments superimposed on the pattern of ODCs. Two main results are apparent. First, there is a tendency for Meynert segments to cross over ODCs. This is especially clear in Fig. 6A, which shows the trajectory of 10 segments in relationship to the ODCs. One of these (green, at the white arrow), originated from a BDA injection in a right eye domain and traveled mainly within a right eye stripe; but eight others from the same injection took an obliquely dorsal trajectory, crossing up to 11 separate ODCs. Another axon (red, at hollow arrow) had two branches which traveled partly parallel to two right eye stripes, but in total still crossed over five domains. In Fig. 5B, four of eight segments run somewhat parallel to the ODCs, but four have an obliquely perpendicular trajectory (higher magnification is shown in Fig. 7). The tendency for crossing over ODCs was also observed in the two other experimental hemispheres.

The second result concerns the distribution of individual terminal clusters relative to the ODCs. Because we utilized serial section reconstruction, these could be unambiguously attributed to single segments (but see "Pitfalls," in Experimental Procedures). As shown in Table 1, terminations distributed to both left- and right-eye columns from most of the segments from the six injection sites. In one case (monkey 22), all eight segments analyzed terminated preferentially in the ODCs contralateral to the injection. For the other three hemispheres (five injections), the results were mixed, but with a slight overall bias for the contralateral eye. For six of 35 segments, boutons were exclusively directed to ipsilateral ($n=5$) or contralateral ODCs ($n=1$); but for these segments the number of boutons within the field was very small. In Fig. 8, the total number of boutons, distributed in left eye and right eye ODCs, has been plotted for 32 segments (B2 and B6 from R18, and B7 from R22 were excluded because of the very small number of total boutons). When these are grouped according to left- or right-eye injections, no significant bias is apparent for terminations in ipsi- or contralateral ODCs. (The ratio was compared between the numbers of boutons ipsi- and contralateral to the injection sites, and was found to be not significantly different from 1. For right ODC injections: Student's *t*-test, $P>0.6$. For left ODC injections: Student's *t*-test, $P>0.3$.)

Terminations occurred both at the borders and in the center of ODCs, without any discernible preference, and could be found in up to three cycles of ODCs. Different spatial distributions occurred: 1) in register across several ODCs (for example, the pink axon in Fig. 6A); 2) offset across several ODCs (for example, the blue axon in Fig. 7A and the white axon in Fig. 7C); or 3) could extend for

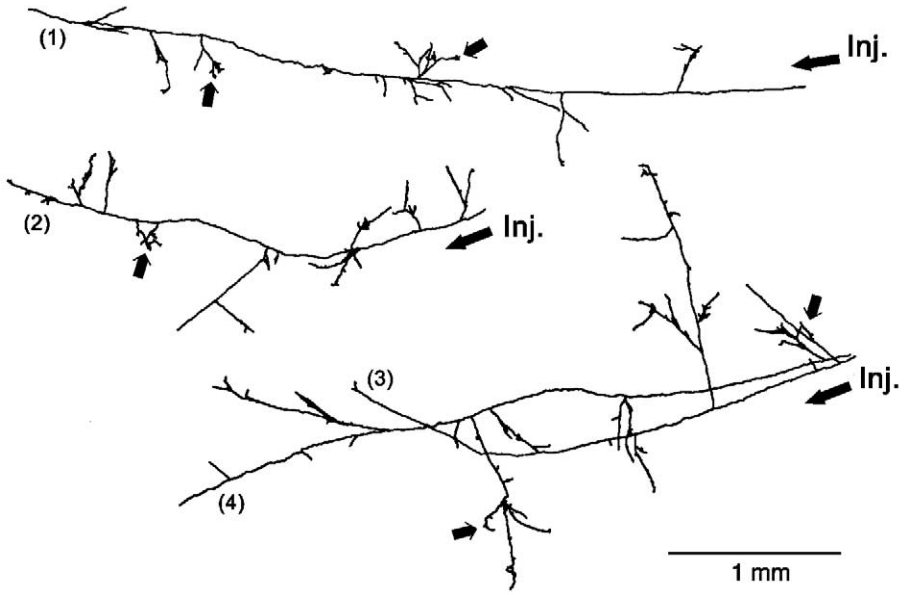

Fig. 5. Distal portions of five Meynert segments. Segments originate from injection site (from the direction of the large solid arrows). Multiple small terminal clusters occur along the axons. Five of these are indicated by small arrows (See also Fig. 7B, C).

1.0–2.0 mm along a single ODC (upper red axon in Fig. 6A, green axon in Fig. 7A, white axon in Fig. 7C).

Commonly, there is a gap of at least 500 μm between the parent cell (in this case, within the injection site), and the first terminal cluster (Figs. 3, 5; and Fig. 12 in Rockland and Knutson, 2001). As shown in Fig. 6, the first cluster can be distant from the soma (within the injection site) by three to five ocular dominance pairs or hypercolumns, and thus is at a distinctly different visual field location from the parent cell body.

DISCUSSION

By using combined optical imaging and single axon reconstruction, we have established two main points. First, we have determined that Meynet cell collaterals commonly cross over ODCs and innervate at least two right- and left-eye pairs or hypercolumns. A previous report showed that Meynert collaterals are very widespread (Rockland and Knutson, 2001); but without the functional imaging, it had been unclear whether segments were aligned mainly within or across ODCs. That is, did the widespread collaterals extend preferentially parallel to the horizontal meridian of the visual field, possibly even within a single ODC? (This might have been suggested by the anterior–posterior orientation of the segments in Fig. 10 of Rockland and Knutson, 2001.) The present study shows that this is not the case, at least for parafoveal vision, and that a single collateral segment has terminations both within and across columns (Fig. 9).

A second result is that Meynert collaterals terminate in both right- and left-eye columns. In one hemisphere (monkey 22), there was some bias in favor of the ODCs ipsilateral to the injection site; but this was less clear in the other three hemispheres. The binocular trend may be viewed as consistent with previous observations that Meynert cells tend to be situated beneath the low CO, interpatch matrix, corresponding to the binocular edges of ODCs (Fries, 1986; Payne and Peters, 1989; Shipp and Zeki, 1989; Boyd and Casagrande, 1999). In the case of the terminations, we could not ascertain any marked preference for the border or centers of ODCs; but this may be because dendrites of postsynaptic neurons undoubtedly extend through both border and center regions.

In considering these results, one question is how they accord with the functional properties of Meynert cells. These neurons have been difficult to investigate because of their sparse distribution (variously estimated as 19–25 cells under 1 mm; Winfield et al., 1981; Payne and Peters, 1989). They are frequently associated with motion processing because of their projections to area MT/V5 and, often via collateral branches, to the superior colliculus (Fries et al., 1985; Vogt Wiesenhorn et al., 1995); and they have been used in at least one model of disparity detection (Livingstone, 1998). One study in cat identifies a putative Meynert neuron as having a very large, binocularly driven standard complex receptive field (Gabbott et al., 1987). The widespread distribution of Meynert collaterals and their termination in both sets of ODCs is suggestive of an involvement with binocular interactions over wide sectors of the visual field. This could be related to several perceptual processes, such as stereopsis or the analysis of optic flow generated by self-movements (e.g. Shipp and Zeki, 1989). The widespread distribution in particular might imply a contribution to perceptual completion and interpolation between illusory contours. The mechanisms underlying long-range linking have been attributed to feedback from higher cortical areas (Grill-Spector and Malach, 2001), or to cascades of lateral intrinsic connections (Pillow and Rubin, 2002); but Meynert

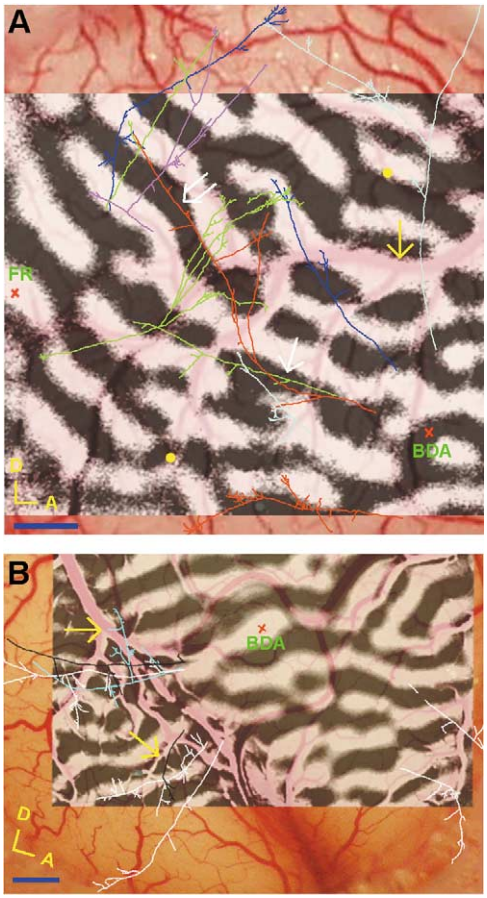

Fig. 6. Alignment of Meynert segments with ODCs. A) Injections of BDA (X) and FR (X) were made, respectively, in a right-eye and left-eye ODC. Six segments from the BDA site and four from the FR site were reconstructed, reduced in size, and aligned onto the ODC maps. Alignment was achieved by reference to the blood vessel pattern and to three DiI fiducial injections, two which are shown as small yellow circles. The field is from the left hemisphere of R19. See text for explanation of white arrows. B) One injection of BDA (X) was placed in a left eye ODC. Eight segments were used in the analysis. The field is from the right hemisphere of R22. Yellow arrows indicate portions shown at higher magnification in Fig. 7. D, dorsal; A, anterior. Scale bars in A, B=1.0 mm.

collaterals would be another candidate for processes requiring long distance interactions, since they can even cross over the horizontal meridian representation (Fig. 5–7 in Rockland and Knutson, 2001).

In continuing work, it will be important to have more information about Meynert cells at the level of their microcircuitry; that is, the source and configuration of inputs, intrinsic membrane properties, and local postsynaptic populations and effects. From the location of these cells at the border of layers 5 and 6, we can suppose that inputs are from geniculocortical collaterals (Blasdel and Lund, 1983), feedback from MT/V5 and other extrastriate areas (Rockland and Knutson, 2001), and/or other neurons in the deeper layers. Concerning their outputs, Meynert collaterals are unlikely to project heavily to layer 4, since their terminations are beaded, not spiny, as has been reported for layer 6 terminations in layer 4 (Fitzpatrick et al., 1985;

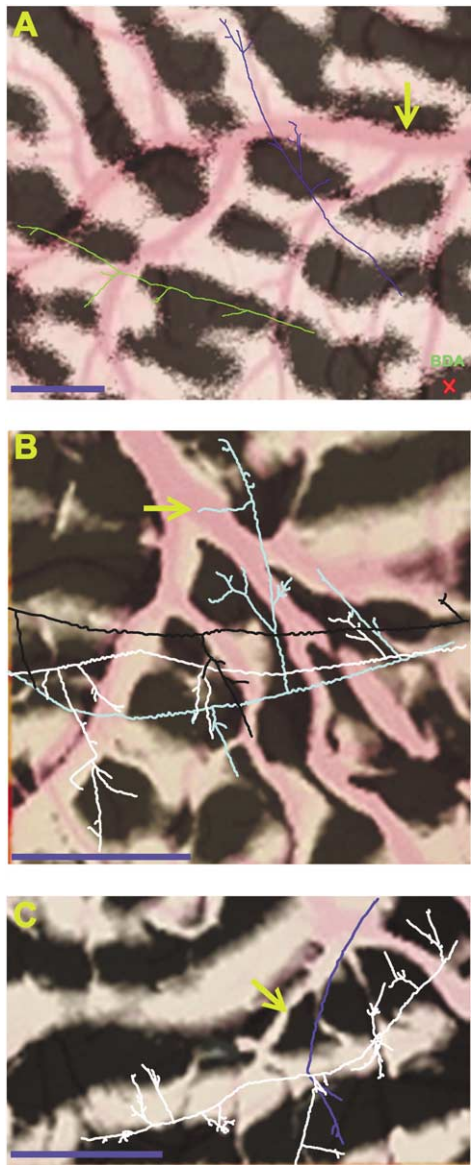

Fig. 7. Enlarged views to show details of the alignment between ODCs and Meynert segments. A) (from yellow arrow in 6A) The purple axon (labeled by the BDA injection in a right ODC) crosses obliquely over four ODCs, and gives off terminal clusters corresponding to right and left ODCs. The green axon runs parallel within a right ODC. For this segment, three of four terminal clusters lie within the right ODC, but a fourth cluster extends between a right and left ODC. B) (From upper arrow in 6B). In this field, the main portion of three axons (labeled by an injection in a left ODC) travel parallel to the ODCs. Both the blue and white axons, however, have perpendicular branches which cross over sets of ODCs. The blue axon has multiple terminal clusters, which are all mainly in right ODCs. The white axon also has multiple clusters, which mainly correspond to right ODCs. The black axon in this enlarged field has three clusters. One of these corresponds to a left ODC, one to a right ODC, and one extends between a left and right ODC. C) (From the lower arrow in 6B). The purple axon takes a course obliquely perpendicular to the ODCs. It has one cluster in this field which corresponds to a right eye ODC. The white axon runs rather parallel to a left eye ODC. It has 10 terminal clusters, which are mixed between both right and left ODCs. Five clusters are entirely or mainly within a right (black) ODC, two are mainly within a left (white) ODC, and three appear to be at the edge of a white and black ODC. Terminations contact two right ODCs.

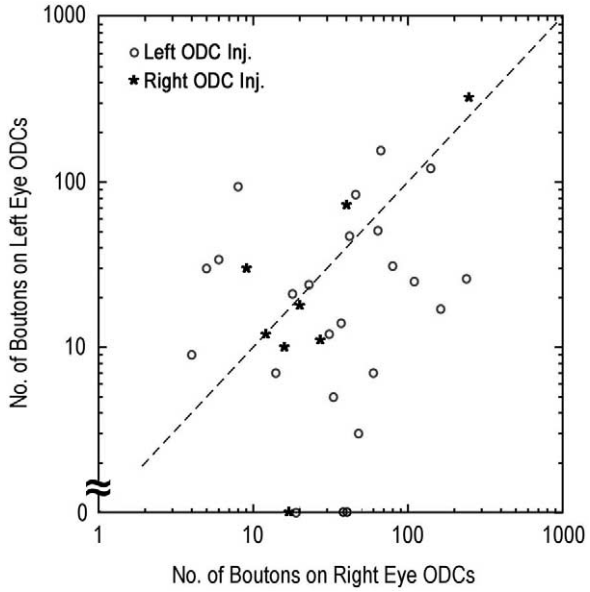

Fig. 8. Logarithmic plot of the number of boutons in left (*y* axis) or right (*x* axis) ODCs, for 32 of the 35 segments in Table 1. Bouton number is shown for eight segments from right ODCs (asterisk) and for 24 segments from left ODCs (open circles). Points above and below the oblique dotted line indicate segments that have more boutons in left ODCs and in right ODCs, respectively. The nearly symmetrical distribution of points against the dotted line indicates that there is no strong tendency for specificity in left or right ODCs.

Anderson et al., 1993; also see lack of any collaterals to layer 4 in Rockland and Knutson, 2001). Since terminal clusters frequently extend into layer 5, the local postsynaptic population is most likely to be corticocollicular neurons and possibly other Meynert cells in the deeper layers.

Another issue is how the system of Meynert collaterals compares with the supragranular intrinsic connections. In particular, the binocular termination pattern is in contrast with reports that the horizontal intrinsic connections of neurons in the supragranular layers terminate preferentially in the same functional compartment, orientation or ocular dominance, as the injection site.

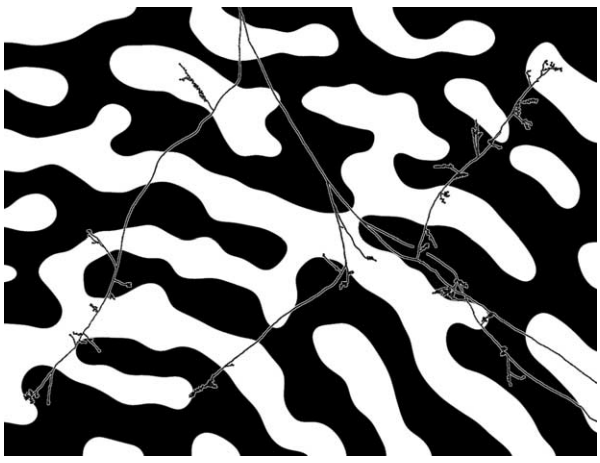

Fig. 9. Schematic summary of a Meynert cell intrinsic collateral mapped against ODCs. Five segments are shown, three of which obliquely cross the field of ODCs. Terminal clusters contact both left- and right-eye ODCs. The parent cell body would be off the image, at the top.

According to Yoshioka et al. (1996), 71% of labeled patches in layer 3 terminate in the same CO compartment as the injection site, 11% in the opposite compartment, and 18% at borders. In relation to ODCs, these investigators found that 54% of labeled patches coincided with same eye ODCs, 28% with opposite eye, and 18% with border regions. Malach et al. (1993) reported that monocular regions were interconnected in a "quasi-specific" manner with same-eye ODCs (67%), and observed that binocular regions, at the borders of ODCs, were selectively interconnected among themselves. A more recent study used GFP adenovirus as an anterograde tracer, in combination with optically imaged orientation domains, and confirmed the overall pattern of like-to-like connectivity for neurons in layer 3 (Stettler et al., 2002).

This apparent difference raises the question of whether the infragranular layers are less tightly linked to the overall functional architecture of V1 than has been demonstrated for the supragranular layers. Some further evidence for this possibility comes from several studies correlating the location of retrogradely filled projection neurons with ODCs or CO compartments. Wiser and Callaway (1997) matched the axonal arbor of 27 biocytin-filled layer 6 neurons with ODCs in cortical slice. They concluded that only three of 27 neurons (corresponding to a particular subtype) showed any marked termination preference in relation to ODCs. Sincich and Horton (2002) reported that neurons projecting to V2 from layers 3 or 4B form patches that correlate with CO patches or interpatches, but that those in layer 5 do not. Boyd and Casagrande (1999) reported, in owl monkey and bushbaby, that neurons projecting to MT/V5 from layer 4B tend to be situated below CO patches, but that the deeper Meynert cell bodies, as reported by others (Fries, 1986; Payne and Peters, 1989; Shipp and Zeki, 1989), may avoid the overlaying CO patches. (But see Krubitzer and Kaas, 1989; Shipp and Zeki, 1989, who did not find any regular mapping of MT-projecting neurons in layer 4B). In addition, no periodicity has yet been revealed for corticogeniculate neurons in layer 6.

The termination-free zone around the Meynert cell body is another point of difference, since, for supragranular pyramidal neurons, the peri-soma home column has the highest terminal density. It is interesting that a comparatively termination-sparse perisomatic zone has also been observed for large basket cells in cat area 18 (Fig. 10 of Buzás et al., 2001); and these, in contrast with small or medium basket cells, also have terminal fields with nearly equal input to right and left eye ODCs.

Acknowledgements—We would like to thank Michiko Fujisawa for assistance with manuscript preparation, and Adrian Knight for assistance with Fig. 9. This work was supported by research funds from RIKEN Brain Science Institute.

REFERENCES

Anderson JC, Martin KAC, Whitteridge D (1993) Form, function, and intracortical projections of neurons in the striate cortex of the monkey *Macacus nemestrinus*. Cereb Cortex 3:412–420.

Blasdel GG (1992) Differential imaging of ocular dominance and orientation selectivity in monkey striate cortex. J Neurosci 12:3115–3138.

Blasdel GG, Lund JS (1983) Termination of afferent axons in macaque striate cortex. J Neurosci 3:1389–1413.

Blasdel GG, Salama G (1986) Voltage sensitive dyes reveal a modular organization in monkey striate cortex. Nature 321:429–431.

Boyd JD, Casagrande VA (1999) Relationships between cytochrome oxidase (CO) blobs in primate primary visual cortex (V1) and the distribution of neurons projecting to the middle temporal area (MT). J Comp Neurol 409:573–591.

Buzás P, Eysel U, Adorjan P, Kisvarday ZF (2001) Axonal topography of cortical basket cells in relation to orientation, direction, and ocular dominance maps. J Comp Neurol 437:259–285.

Cheng K, Waggoner RA, Tanaka K (2001) Human ocular dominance columns as revealed by high-field functional magnetic resonance imaging. Neuron 32:359–374.

DeYoe EA, Van Essen DC (1988) Concurrent processing streams in monkey visual cortex. Trends Neurosci 11:219–226.

Fitzpatrick D, Lund JS, Blasdel GG (1985) Intrinsic connections of macaque striate cortex: afferent and efferent connections of lamina 4C. J Neurosci 5:3329–3349.

Fries W (1986) Distribution of Meynert cells in primate striate cortex: spatial relationships with cytochrome oxidase blobs. Naturwissenschaften 73:557–558.

Fries W, Keizer K, Kuypers HG (1985) Large layer V1 cells in macaque striate cortex (Meynert cells) project to both superior colliculus and prestriate area V5. Exp Brain Res 58:613–616.

Gabbott PLA, Martin KAC, Whitteridge D (1987) Connections between pyramidal neurons in layer 5 of cat visual cortex (area 17). J Comp Neurol 259:364–381.

Grill-Spector K, Malach R (2001) fMR-adaptation: a tool for studying the functional properties of human cortical neurons. Acta Psychol (Amst) 107:293–321.

Grinvald A, Frostig RD, Siegel RM, Bartfeld E (1991) High-resolution optical imaging of functional brain architecture in the awake monkey. Proc Natl Acad Sci USA 88:11559–11563.

Hubel DH, Wiesel TN (1968) Receptive fields and functional architecture of monkey visual cortex. J Physiol 195:215–243.

Hubel DH, Wiesel TN (1972) Laminar and columnar distribution of geniculo-cortical fibers in the macaque monkey. J Comp Neurol 146:421–450.

Hubel DH, Wiesel TN (1977) Functional architecture of macaque monkey visual cortex. Proc R Soc Lond B Bio Sci 198:1–59.

Li HB, Fukuda M, Tanifuji M, Rockland KS (2000) Correlation of Meynert cell intrinsic collaterals with ocular dominance columns in monkey primary visual cortex. Soc Neurosci Abstr 26:143.

Li HB, Fukuda M, Tanifuji M, Rockland KS (2001) Relationship between intrinsic collaterals of layer VI Meynert cells and functional columns in primate V1. Soc Neurosci Abstr 285.9.

Livingstone MS (1998) Mechanisms of direction selectivity in macaque V1. Neuron 20:509–526.

Livingstone MS, Hubel DH (1983) Specificity of cortico-cortical connections in monkey visual system. Nature 304:531–534.

Malach R, Amir Y, Harel M, Grinvald A (1993) Relationship between intrinsic connections and functional architecture revealed by optical imaging and in vivo targeted biocytin injections in primate striate cortex. Proc Natl Acad Sci USA 90:10469–10473.

Movshon JA, Newsome WT (1996) Visual response properties of striate cortical neurons projecting to area MT in macaque monkeys. J Neurosci 16:7733–7741.

Payne BR, Peters A (1989) Cytochrome oxidase patches and Meynert cells in monkey visual cortex. Neuroscience 28:353–363.

Pillow J, Rubin N (2002) Perceptual completion across the vertical meridian and the role of early visual cortex. Neuron 33:805–813.

Rockland KS, Lund JS (1983) Intrinsic laminar lattice connections in primate visual cortex. J Comp Neurol 216:303–318.

Rockland KS, Knutson T (2001) Axon collaterals of Meynert cells diverge over large portions of area V1 in the macaque monkey. J Comp Neurol 441:134–147.

Shipp S, Zeki S (1989) The organization of connections between areas V5 and V1 in macaque monkey visual cortex. Eur J Neurosci 1:309–332.

Shtoyerman E, Arieli A, Slovin H, Vanzetta I, Grinvald A (2000) Long-term optical imaging and spectroscopy reveal mechanisms underlying the intrinsic signal and stability of cortical maps in V1 of behaving monkeys. J Neurosci 20:8111–8121.

Sincich L, Horton JC (2002) Divided by cytochrome oxidase: a map of the projections from V1 to V2 in macaques. Science 295:1745–1737.

Stettler DD, Das A, Bennett J, Gilbert CD (2002) Lateral connectivity and contextual interactions in macaque primary visual cortex. Neuron 36:739–750.

Ts'o DY, Frostig RD, Lieke EE, Grinvald A (1990) Functional organization of primate visual cortex revealed by high resolution optical imaging. Science 249:417–420.

Tsunoda K, Yamane Y, Nishizaki M, Tanifuji M (2001) Complex objects are represented in macaque inferotemporal cortex by the combination of feature columns. Nat Neurosci 4:832–838.

Vogt Weisenhorn DM, Illing R-B, Spatz WB (1995) Morphology and connections of neurons in area 17 projecting to the extrastriate areas MT and 19DM and to the superior colliculus in the monkey *Callithrix jacchus*. J Comp Neurol 362:233–255.

Winfield DA, Rivera-Dominguez M, Powell TPS (1981) The number and distribution of Meynert cells in area 17 of the macaque monkey. Proc R Soc Lond B 213:27–40.

Wiser AK, Callaway EM (1997) Ocular dominance columns and local projections of layer 6 pyramidal neurons in macaque primary visual cortex. Visual Neurosci 14:241–251.

Yabuta NH, Callaway EM (1998) Cytochrome-oxidase blobs and intrinsic horizontal connections of layer 2/3 pyramidal neurons in primate V1. Visual Neurosci 15:1007–1027.

Yoshioka T, Blasdel GG, Levitt JB, Lund JS (1996) Relation between patterns of intrinsic lateral connectivity, ocular dominance, and cytochrome oxidase-reactive regions in macaque monkey striate cortex. Cereb Cortex 6:297–310.

(Accepted 21 May 2003)